

Displacement eigenmodes for cold-fluid and warm-fluid magnetized plasma oscillations

Daniel H. E. Dubin

Department of Physics, University of California at San Diego, La Jolla, California 92093

(Received 14 October 2004; accepted 6 December 2004; published online 24 March 2005)

Cold-fluid and warm-fluid electrostatic plasma modes of magnetized nonuniform plasmas are determined as eigenfunctions of an integral equation describing the perturbed fluid displacement. The frequencies of these displacement eigenmodes are always real. In some cases, the modes are singular and form a continuous spectrum, and this causes spatially Landau-damped quasimodes to appear in the response to initial perturbations. In other cases the spectrum is discrete. Finite-temperature frequency shifts, of interest as a temperature diagnostic, are evaluated and compared to analytic theory. © 2005 American Institute of Physics. [DOI: 10.1063/1.1854153]

I. INTRODUCTION

This paper examines linear electrostatic plasma oscillations in inhomogeneous magnetized plasmas, using cold-fluid and warm-fluid theory. Linear fluid theory for electrostatic plasma modes in a bounded plasma is often formulated as a differential equation for the plasma potential^{1–3} or, equivalently, the electric field. Here, by introducing a Green's function for the potential, the theory is recast as an integral equation for the perturbed fluid displacement along the magnetic field. The approach is similar to that taken by Case and Van Kampen in formulating the kinetic theory of plasma waves as an integral equation for the velocity distribution function.^{4,5} Our approach is particularly useful when cross-magnetic-field drift motion can be ignored in the wave dynamics, as is assumed here.

Our integral equation involves a linear operator \hat{A} that we refer to as the *acceleration operator*. The action of this operator on a given fluid displacement yields the acceleration associated with this displacement. An eigenmode of the system with frequency ω is an eigenfunction of this operator, with real eigenvalue $-\omega^2$; i.e., it is a special fluid displacement (a *displacement eigenmode*) for which the corresponding acceleration has the same functional form, except for a constant of proportionality equal to $-\omega^2$.

This approach has several advantages: the acceleration operator is Hermitian, so the displacement eigenmodes form a complete orthogonal set. Any initial value problem can be solved using a superposition of these eigenmodes. Also, since the eigenfrequencies can be easily found numerically from the eigenvalues of a matrix, one can determine the evolution of perturbations about arbitrary plasma equilibria, including finite-temperature corrections. Furthermore, the displacement eigenmodes are only required inside the plasma, so vacuum regions surrounding the plasma need not be treated. This simplifies the numerics.

The approach is applied to determine eigenmodes for several different equilibria. For the case of plasma pancakes (i.e., slab geometry) with continuously varying equilibrium density $n_0(z)$, we find that in cold-fluid theory the spectrum of displacement eigenmodes is continuous and the eigen-

modes are singular, resulting in spatial Landau damping of initial perturbations. The physical mechanism of the damping is emission of magnetized plasma waves at a resonance layer. This collisionless damping mechanism is well known.^{6–8}

However, when warm-fluid effects are added to the eigenmode dynamics, and when $n_0(z)$ is given by the thermal equilibrium density profile associated with a non-neutral plasma, the spectrum is discrete and there is no spatial Landau damping.

On the other hand, for spherical non-neutral plasmas in thermal equilibrium at finite temperature, we again find a continuous spectrum of singular displacement eigenmodes, resulting in spatial Landau damping. The physical mechanism of the damping again appears to be emission of magnetized plasma waves at a resonance layer, in close analogy to the mechanism of collisionless damping in unmagnetized fluid plasmas,^{6–8} although several aspects of the process are not yet well understood.

For both slab and spherical geometries finite-temperature mode frequency shifts, which can be used as a temperature diagnostic,^{9,10} are compared to results of perturbation theory¹¹ for the frequency shifts, and the perturbation theory is shown to work well for sufficiently low temperatures.

In Sec. II we develop the general theory of displacement eigenmodes. In Sec. III we discuss numerical methods for evaluation of the eigenmodes, and examine the results of these evaluations in slab and spherical thermal equilibria. Section IV summarizes the results and discusses several open questions.

II. GENERAL THEORY

We first review the warm-fluid description of electron plasma waves in an inhomogeneous magnetized plasma, and then derive the equations describing displacement eigenmodes. Assuming that the magnetic field is uniform, $\mathbf{B} = B\hat{z}$, these magnetized plasma waves are described by the following momentum, continuity, and Poisson equations:

$$m_e n_e \frac{d^2 Z}{dt^2} = en_e \frac{\partial \phi}{\partial z} - \frac{\partial p}{\partial z}, \quad (1)$$

$$\frac{\partial n_e}{\partial t} + \frac{\partial}{\partial z} \left(n_e \frac{\partial Z}{\partial t} \right) = 0, \quad (2)$$

$$\nabla^2 \phi = 4\pi e(n_e - n_b), \quad (3)$$

where $Z(\mathbf{r}, t)$ is the axial displacement of a fluid element, $n_e(\mathbf{r}, t)$ and $p(\mathbf{r}, t)$ are the electron density and pressure, respectively, $\phi(\mathbf{r}, t)$ is the electrostatic potential, and $n_b(\mathbf{r})$ is a static background charge, provided either by ions or by rotation through the magnetic field (as in the case of a non-neutral plasma). Only displacements along the magnetic field are kept in Eqs. (1) and (2): the plasma is assumed to be in the regime $\omega_p \ll \Omega_c$ (where ω_p and Ω_c are the electron plasma and cyclotron frequencies, respectively), so that $\mathbf{E} \times \mathbf{B}$ drifts and cyclotron motion are neglected.

In equilibrium, the electron density $n_0(\mathbf{r})$, pressure $p_0(\mathbf{r})$, and potential $\phi_0(\mathbf{r})$ satisfy time-independent limits of Eqs. (1)–(3),

$$0 = en_0 \frac{\partial \phi_0}{\partial z} - \frac{\partial p_0}{\partial z}, \quad (4)$$

$$\nabla^2 \phi_0 = 4\pi e(n_0 - n_b), \quad (5)$$

and these, together with an ideal-gas equation of state

$$p_0 = n_0 T, \quad (6)$$

allow one to uniquely determine the plasma equilibrium, given the boundary conditions on the potential. In what follows we will assume that the electron temperature T is uniform.

Equations describing small perturbations away from this equilibrium are found by subtracting Eqs. (4) and (5) from Eqs. (1) and (3) and linearizing, writing $\phi = \phi_0 + \delta\phi$, $n_e = n_0 + \delta n$, $p = p_0 + \delta p$, and $Z = \delta Z$.

These perturbations are assumed to have time dependence of the form $e^{-i\omega t}$. The resulting linearized fluid equations are

$$-m_e n_0 \omega^2 \delta Z = en_0 \frac{\partial \delta\phi}{\partial z} + e \delta n \frac{\partial \phi_0}{\partial z} - \frac{\partial \delta p}{\partial z}, \quad (7)$$

$$\delta n + \frac{\partial}{\partial z} (n_0 \delta Z) = 0, \quad (8)$$

$$\nabla^2 \delta\phi = 4\pi e \delta n. \quad (9)$$

In addition, an adiabatic equation of state for the pressure perturbations is employed: $d(p/n_e^\gamma)/dt = 0$, where $\gamma = 3$ is the ideal-gas ratio of specific heats for 1 D motions along the magnetic field. Linearization of this equation yields

$$\delta p = -\delta Z \frac{\partial p_0}{\partial z} - \gamma p_0 \frac{\partial \delta Z}{\partial z}. \quad (10)$$

These equations can be reduced by combining Eqs. (4), (6), (8), and (10) with Eq. (7):

$$-\omega^2 \delta Z = \frac{e}{m_e} \frac{\partial \delta\phi}{\partial z} + \bar{v}^2 \frac{\partial^2 \ln n_0}{\partial z^2} \delta Z + \frac{\gamma \bar{v}^2}{n_0} \frac{\partial}{\partial z} \left(n_0 \frac{\partial \delta Z}{\partial z} \right), \quad (11)$$

where $\bar{v} = \sqrt{T/m_e}$ is the electron thermal speed, and

$$\nabla^2 \delta\phi = -\frac{\partial}{\partial z} (4\pi e n_0 \delta Z). \quad (12)$$

Equations (11) and (12) form a coupled set for δZ and $\delta\phi$, which may be solved given appropriate boundary conditions. Here we will assume homogeneous Dirichlet conditions on $\delta\phi$. The boundary conditions on δZ depend on the form of the equilibrium density n_0 . Assuming the plasma is contained away from surrounding electrodes so that $n_0 \rightarrow 0$, the singularity in the last term of Eq. (11) implies that the general solution will typically have singular behavior in the vacuum region. An eigenvalue problem can then be specified by simply requiring that δZ remain finite outside the plasma.

For a homogeneous plasma, a dispersion relation follows by assuming perturbed quantities vary as $e^{i\mathbf{k}\cdot\mathbf{r}}$, where \mathbf{k} is the wave number. Equations (11) and (12) then reduce to

$$\omega^2 = \omega_p^2 \frac{k_z^2}{k^2} + \gamma \bar{v}^2 k_z^2, \quad (13)$$

the well-known dispersion relation for magnetized electron plasma waves.¹² However, for a nonuniform plasma Eqs. (11) and (12) must generally be solved numerically.

The approach taken in this paper is to recast these equations in the form of a single integral equation for δZ . This is accomplished by solving Eq. (12) via a Green's function $G(\mathbf{r}, \mathbf{r}')$ that implicitly accounts for the homogeneous boundary conditions imposed on $\delta\phi$:

$$\delta\phi(\mathbf{r}, t) = -4\pi e \int d^3\mathbf{r}' G(\mathbf{r}, \mathbf{r}') \frac{\partial}{\partial z'} [n_0(\mathbf{r}') \delta Z(\mathbf{r}', t)], \quad (14)$$

where G satisfies the homogeneous boundary conditions, and

$$\nabla^2 G(\mathbf{r}, \mathbf{r}') = \delta(\mathbf{r} - \mathbf{r}'). \quad (15)$$

Integrating by parts in Eq. (14) and substituting the result into Eq. (11) leads to an eigenvalue problem

$$-\omega^2 \delta Z = \hat{A} \delta Z, \quad (16)$$

where \hat{A} is an integrodifferential operator, defined below by its action on an arbitrary function $f(\mathbf{r})$:

$$\hat{A}f \equiv \int d^3r' \omega_p^2(\mathbf{r}') \frac{\partial^2 G}{\partial z \partial z'}(\mathbf{r}, \mathbf{r}') f(\mathbf{r}') + \bar{v}^2 \left[\frac{\partial^2 \ln n_0}{\partial z^2} f(\mathbf{r}) + \frac{\gamma}{n_0} \frac{\partial}{\partial z} \left(n_0 \frac{\partial f}{\partial z} \right) \right], \quad (17)$$

and $\omega_p^2(\mathbf{r}) = 4\pi e^2 n_0(\mathbf{r})/m_e$. Thus, normal mode frequencies ω are given by the eigenvalues of the operator \hat{A} , with corresponding eigenfunctions δZ . Physically, this operator yields the acceleration associated with a given displacement from equilibrium, and is therefore referred to as the acceleration operator.

The acceleration operator \hat{A} is Hermitian with respect to the following inner product:

$$(f, g) \equiv \int d^3r f^*(\mathbf{r})g(\mathbf{r})\omega_p^2(\mathbf{r}), \quad (18)$$

where f and g are arbitrary functions. Therefore, eigenfunctions $\delta Z(\mathbf{r})$ of \hat{A} form a complete orthogonal set and eigenvalues ω^2 are real.

This implies that the evolution $\delta Z(\mathbf{r}, t)$ of any initial axial displacement $\delta Z_0(\mathbf{r})$ or initial axial velocity $\delta V_0(\mathbf{r})$ can be written as a superposition of these eigenmodes:

$$\delta Z(\mathbf{r}, t) = \sum_{\omega} \left\{ \begin{array}{l} \frac{(\delta Z_{\omega}, \delta Z_0)}{(\delta Z_{\omega}, \delta Z_{\omega})} \delta Z_{\omega}(\mathbf{r}) \cos \omega t \\ + \frac{(\delta Z_{\omega}, \delta V_0)}{\omega(\delta Z_{\omega}, \delta Z_{\omega})} \delta Z_{\omega}(\mathbf{r}) \sin \omega t \end{array} \right\}, \quad (19)$$

where $\delta Z_{\omega}(\mathbf{r})$ is the eigenmode corresponding to eigenfrequency ω .

It remains only to determine the eigenmodes of \hat{A} . In the following section we evaluate these eigenmodes numerically for several cases, and compare the results to known theory for the modes.

III. DISPLACEMENT EIGENMODES

A. General remarks on the cold-fluid limit

In the cold-fluid limit, the pressure term in Eq. (1) is negligible. Terms in the acceleration operator proportional to thermal speed are dropped, yielding a cold-fluid acceleration operator \hat{A}_0 given by only the first term in Eq. (17):

$$\hat{A}_0 \delta Z = \int d^3r' \omega_p^2(\mathbf{r}') \frac{\partial^2 G}{\partial z \partial z'}(\mathbf{r}, \mathbf{r}') \delta Z(\mathbf{r}'). \quad (20)$$

Cold-fluid eigenmodes can alternately be written as solutions to a differential equation involving the potential rather than the displacement. Using Eqs. (7) and (12), it is easy to show that

$$\omega^2 \nabla^2 \delta \phi = \frac{\partial}{\partial z} \left(\omega_p^2 \frac{\partial \delta \phi}{\partial z} \right). \quad (21)$$

This form of the eigenvalue problem has the advantage that it is local as opposed to the integral operator \hat{A}_0 . On the other hand, it is not a standard eigenvalue problem, but rather a generalized eigenvalue problem requiring somewhat more complex numerical methods to determine the eigenmodes.² Also, unlike displacement eigenmodes, the potential eigenfunctions do not form a complete orthogonal basis. This creates difficulties when evaluating the time-dependent response to an initial perturbation, since there is no expansion involving $\delta \phi$ that is equivalent to Eq. (19).

Nevertheless, a useful analytic result follows from the simple form of Eq. (21): one can show that eigenfrequencies fall in the range $0 < \omega^2 < \text{Max}(\omega_p^2)$. By application of $\int d^3r \delta \phi^*$ to both sides of Eq. (21), an integration by parts then yields

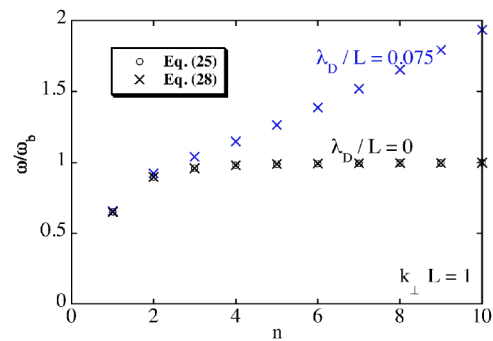


FIG. 1. (Color online). Cold-fluid and warm-fluid normal mode frequencies for $k_{\perp}L=1$. The integer n enumerates the modes in order of their frequencies. Circles are solutions of Eq. (25), crosses are from discretized displacement eigenmodes, Eq. (28). For $\lambda_D/L=0$, cold-fluid dynamics is used and the equilibrium is a uniform plasma slab of thickness $2L$ (a top-hat profile). For $\lambda_D/L=0.075$, warm-fluid dynamics is used and the equilibrium is the corresponding thermal equilibrium profile (see Fig. 3).

$$\int d^3r \omega^2 |\nabla_{\perp} \delta \phi|^2 + (\omega^2 - \omega_p^2) |\partial \delta \phi / \partial z|^2 = 0, \quad (22)$$

where $\nabla_{\perp} = (\partial/\partial x, \partial/\partial y)$. It is only possible to satisfy this equation if the second term is negative over some region of \mathbf{r} , which implies that $\omega^2 < \text{Max}(\omega_p^2)$. On the other hand, if $\omega^2 < 0$, then the integrand is everywhere negative, which also prohibits a solution. Therefore, $0 < \omega^2 < \text{Max}(\omega_p^2)$.

B. Slab geometry

1. Cold-fluid limit, top-hat profile

As a first test of the displacement eigenmode method, we will consider a top-hat profile for which

$$\begin{aligned} \omega_p(z) &= \omega_b \quad |z| < L \\ &= 0, \quad |z| > L, \end{aligned} \quad (23)$$

where ω_b is a constant plasma frequency.

For a uniform-density plasma slab in free space, running from $-L < z < L$, the solution of Eq. (21) for the potential eigenmodes breaks into even and odd modes. Inside the plasma, this mode potential has the form

$$\delta \phi(\mathbf{r}) = \frac{\sin}{(\cos)} [k_{\perp} z / \varepsilon(\omega)] e^{i\mathbf{k}_{\perp} \cdot (x, y)} \quad (24)$$

with frequencies satisfying

$$f(\omega) = 0, \quad (25a)$$

where

$$f(\omega) = \frac{1}{\varepsilon(\omega)} \tan\left(\frac{k_{\perp} L}{\varepsilon(\omega)}\right) - 1 \quad (25b)$$

for $\delta \phi$ odd in z ,

$$f(\omega) = \varepsilon(\omega) \tan\left(\frac{k_{\perp} L}{\varepsilon(\omega)}\right) + 1 \quad (25c)$$

for $\delta \phi$ even in z , and where $\varepsilon(\omega) = \sqrt{\omega_b^2 / \omega^2 - 1}$. For given $k_{\perp} L$, Eq. (25a) can be solved numerically. Examples are shown in Fig. 1 for $k_{\perp} L = 1$ (the circles). Here, the positive integer n counts the modes in order of their frequency.

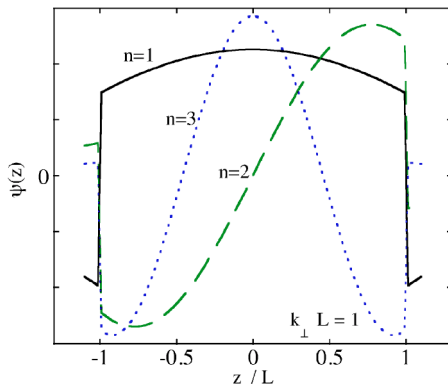


FIG. 2. (Color online). The first three cold-fluid displacement eigenmodes for a uniform plasma slab (a top-hat profile), assuming $k_{\perp}L=1$.

In order to solve this problem using the displacement eigenmodes for a plasma slab, we first note that the Green's function for perturbations of the form $\delta Z(\mathbf{r}) = \psi(z)e^{i\mathbf{k}_{\perp} \cdot (x,y)}$ can be written as

$$G(\mathbf{r}, \mathbf{r}') = -\frac{e^{i\mathbf{k}_{\perp} \cdot [(x,y)-(x',y')]} }{2k_{\perp}} e^{-k_{\perp}|z-z'|}. \quad (26)$$

Using this result in Eq. (20) implies that cold-fluid displacement eigenmodes of a plasma slab satisfy

$$-\omega^2 \psi(z) = -\omega_p^2(z) \psi(z) + \int dz' \frac{k_{\perp}}{2} e^{-k_{\perp}|z-z'|} \omega_p^2(z') \psi(z'). \quad (27)$$

We solve for the eigenmodes numerically by discretizing $\psi(z)$ on a uniform grid $z_j = z_0 + j\Delta z$, $0 \leq j \leq M$. Then Eq. (20) becomes

$$-\omega^2 \psi_j = A_{jk} \psi_k, \quad (28)$$

where the matrix A_{jk} is a discretized form of \hat{A}_0 :

$$A_{jk} = -\omega_p^2(z_j) \delta_{jk} + \frac{k_{\perp} \Delta z}{2} e^{-k_{\perp}|z_j - z_k|} \omega_p^2(z_k). \quad (29)$$

Note that a grid is needed only where $\omega_p^2(z)$ is nonzero: there is no need to deal with vacuum regions outside the plasma, since boundary conditions are already built into the Green's function. Also, A_{jk} is Hermitian with respect to the finite-differenced inner product $(f, g) = \sum_j f_j^* g_j \omega_p^2(z_j)$, so ω^2 must be real.

Numerical error in the eigenfrequencies and eigenfunctions is introduced by this discretization, but can be minimized if z_0 and Δz are chosen appropriately. Taking $z_0 = -L + \Delta z/2$ and $\Delta z = 2L/(M+1)$ yields a symmetric grid that is matched to the sharp plasma boundary, and for which the discretization error is of $O[(\Delta z/L)^2]$. Other nonoptimal grid choices do not necessarily match the sharp boundary and yield larger errors of $O(\Delta z/L)$. Even so, for sufficiently fine grid the method works admirably. Examples are displayed in Figs. 1 and 2 assuming $k_{\perp}L=1$, and for an unoptimized grid, taking $M=100$ and $z_0 = -1.1L$, and $\Delta z = 2|z_0|/M$ which includes a small vacuum region outside the plasma. Even with this poor grid choice, frequencies match the expected theory

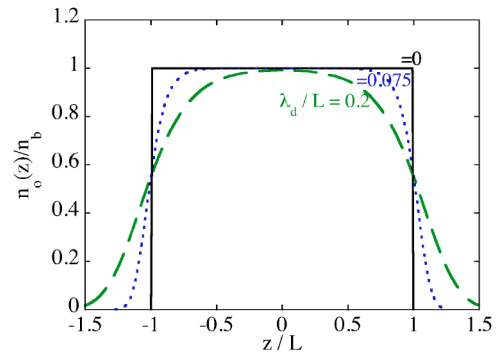


FIG. 3. (Color online). Thermal equilibrium density profile for three temperatures: $\lambda_D/L=0$ (a top-hat profile given by the solid line), $\lambda_D/L=0.075$ (dotted line), $\lambda_D/L=0.2$ (dashed line).

result for $k_{\perp}L=1$ to an accuracy of a few parts in 10^{-4} . The eigenfunctions for the lowest three modes are displayed in Fig. 2. These also closely match the expected form given by Eq. (24).

The lowest frequency ($n=1$) mode represents a “drum-head” type of displacement, where the slab as a whole is displaced in z as $e^{i\mathbf{k}_{\perp} \cdot (x,y) - i\omega t}$. The $n=2$ mode is a “breathing mode” where the slab expands and contracts. Increasing n corresponds to shorter axial wavelength and higher frequency, approaching ω_b , as expected qualitatively from the cold-fluid limit of the homogeneous dispersion relation, Eq. (13).

2. Cold-fluid limit, continuous profile

Next, we consider a continuous density profile. Although any density dependence could in principle be chosen, we focus here on thermal equilibrium profiles associated with non-neutral plasmas,¹³ since they are of current experimental interest.^{9,10,14} The thermal equilibrium density $n_0(z)$ satisfies Eqs. (4)–(6), yielding the following equations for $\omega_p^2(z) = 4\pi e^2 n_0(z)/m_e$:

$$\omega_p^2(z) = \omega_b^2 e^{\chi(z)}, \quad (30)$$

where $\chi(z)$ satisfies

$$\lambda_D^2 \frac{d^2 \chi}{dz^2} = e^{\chi} - 1, \quad \chi'(0) = 0, \quad \chi(0) = -\varepsilon, \quad (31)$$

and where $\lambda_D = \sqrt{T/4\pi e^2 n_b}$ is the constant Debye length associated with the uniform background density n_b , $\omega_b^2 = 4\pi e^2 n_b/m_e$, and ε is chosen so that

$$\int_{-\infty}^{\infty} dz n_0(z) = 2Ln_b. \quad (32)$$

This constraint keeps the total particle number fixed as temperature varies.

Normalizing $n_0(z)$ to n_b , and normalizing distances to L , Eqs. (31) and (32) may be seen to depend on a single parameter, λ_D/L . We solve these equations numerically. For $\lambda_D/L=0.075$, $n_0(z)$ is displayed in Fig. 3. Using these density profiles in Eq. (29), the grid is chosen so that it starts and

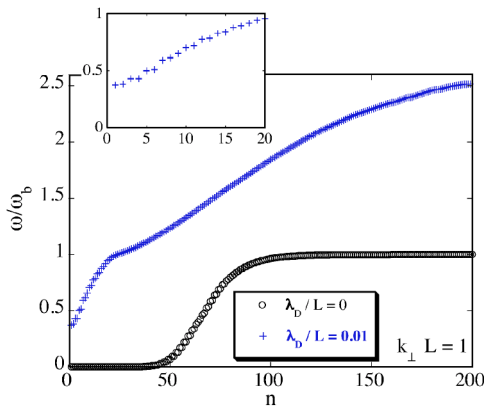


FIG. 4. (Color online). Main plot shows both cold-fluid (circles) and warm-fluid (crosses) displacement mode frequencies for a single equilibrium density profile given by the dotted line in Fig. 3. We take $M=200$, and a grid on $z=-1.5$ to 1.5 . Inset shows the first 20 warm-fluid mode frequencies for dynamics with temperature such that $\lambda_D/L=0.01$, for both $M=200$ and 400 . There is no discernible difference between $M=200$ and $M=400$, indicating that the spectrum is discrete.

ends well outside the plasma; we take $z_0/L=-1.5$ and $\Delta z = 2z_0/M$ for $M=200$. Resulting numerical mode frequencies for $k_{\perp}L=1$ are displayed in Fig. 4.

The cold-fluid displacement mode frequencies now form a continuous spectrum (the circles in Fig. 4). Even more striking differences from the top-hat profile can be seen in the displacement eigenfunctions (Fig. 5), which display singularities at the locations $z=z_r$ where $\omega^2 = \omega_p^2(z_r)$. Physically these singularities arise because an eigenmode with frequency ω resonates with the local plasma frequency $\omega_p(z_r)$. Since these eigenfunctions are singular, they cannot be excited individually. Rather, wave packets of eigenfunctions contribute to the response to initial perturbations, through Eq. (19). For a continuous spectrum, the sum over frequencies in this equation becomes an integral.

Numerical error is introduced through discretization, which turns the integral back into a sum over the numerical eigenmodes. This implies that the numerical solution given by Eq. (19) breaks down for times so large that $e^{i\omega t}$ varies rapidly in ω compared to the frequency difference $\delta\omega$ between adjacent numerical eigenmodes. That is, the numerical solution breaks down for times t such that¹⁵

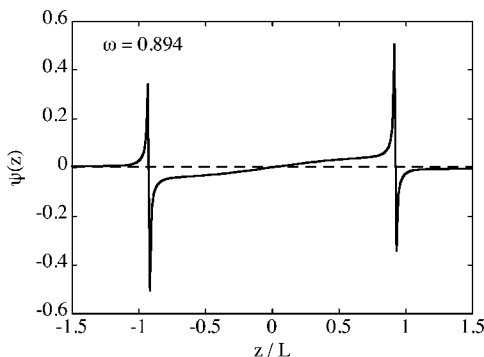


FIG. 5. A cold-fluid displacement eigenmode for the equilibrium density profile given by the dotted line in Fig. 3, assuming $k_{\perp}L=1$. This mode corresponds to the peak of the excitation spectrum shown in Fig. 6.

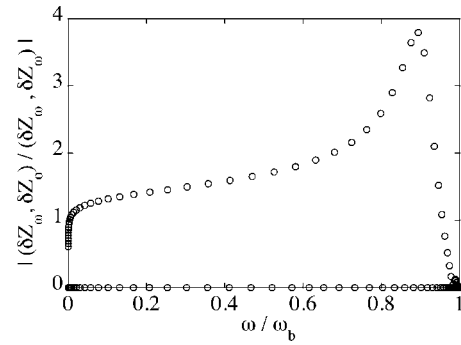


FIG. 6. Excitation spectrum of cold-fluid eigenmodes of the equilibrium density profile given by the dotted line in Fig. 3. The initial condition δZ_0 is an $n=2, k_{\perp}L=1$ top-hat displacement mode [see Fig. 2 and Eq. (19)].

$$\delta\omega_m t \gtrsim 1, \tag{33}$$

where $\delta\omega_m$ is the maximum frequency difference between adjacent eigenmodes in the numerical spectrum. For continuous density profiles, $\delta\omega_m = O(\Delta z)$.

A continuous spectrum indicates the possibility of damped quasimodes in the response of the system to a given initial condition. These quasimodes are wave packets of eigenmodes with a roughly Lorentzian spectral shape centered on top-hat profile mode frequencies. They can be uncovered by using top-hat eigenmodes as initial conditions in Eq. (19). An example is displayed in Figs. 6 and 7. Taking $\delta V_0=0$ and δZ_0 as the top-hat eigenmode for $n=2, k_{\perp}L=1$ (see Fig. 2), the excitation spectrum $(\delta Z_{\omega}, \delta Z_0)/(\delta Z_{\omega}, \delta Z_{\omega})$ is shown in Fig. 6. One can see a peak in this spectrum centered near the cold-fluid frequency for this mode, $\omega/\omega_b = 0.897$.

However, the peak is broadened, which causes spatial Landau damping. A global measure of the overall mode amplitude,

$$\delta\langle z^2 \rangle(t) \equiv \frac{\int dz \delta n(z,t) z^2}{\int dz \delta n(z,0) z^2}$$

is displayed in Fig. 7. This global measure displays the spatial Landau damping associated with a quasimode with

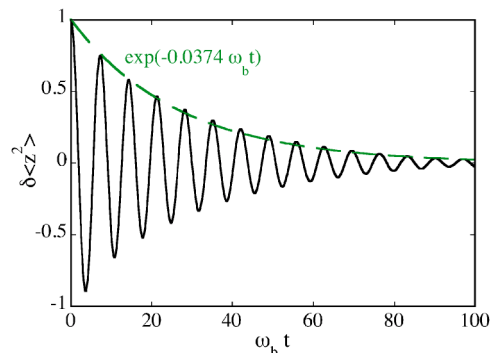


FIG. 7. (Color online). Temporal evolution of $\delta\langle z^2 \rangle$ following from the excitation spectrum shown in Fig. 6.

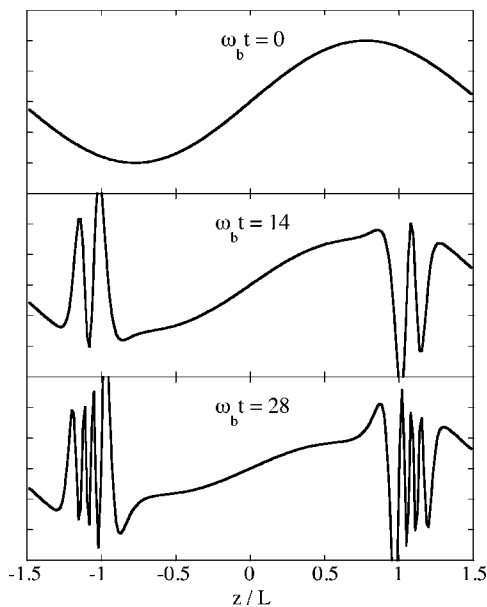


FIG. 8. Cold-fluid displacement $\delta Z(z, t)$ for the $n=2$ quasimode (see Fig. 2) at three times. The plasma equilibrium is taken to be the dotted line in Fig. 3, and $k_{\perp}L=1$ is assumed.

damping rate $\nu/\omega_b=0.0374$. That is, the $n=2$ breathing “mode” is damped, even though all displacement eigenmodes have real frequencies.

In Fig. 8, $\delta Z(z, t)$ is displayed three times, and the physical mechanism of the damping becomes apparent. Filamentary structures form in $\delta Z(z, t)$ around the resonance at $z=z_r$. These structures are localized bulk plasma oscillations that are driven by the global fluid mode.

This spatial Landau damping of the cold-fluid plasma response is well known from the early days of plasma physics.^{6–8} A similar quasimode analysis to that used here has also been applied to spatial Landau damping of diocotron quasimodes.¹⁵ The damping rate of the quasimodes can be determined by the method of contour deformation (see Appendix A) with the result that, for weakly damped modes, the complex quasimode frequency ω is given by the solution to

$$f(\omega) = -\frac{i\pi\omega_0^2 k_{\perp}}{|\partial\omega_p^2/\partial z|_{z=z_r}}, \quad (34)$$

where ω_0 is the real solution to the top-hat mode equation, Eq. (25). According to this equation, the low-order quasimodes with the lowest real frequencies have resonances at the plasma edge where $\partial\omega_p^2/\partial z|_{z=z_r}$ is large, and therefore are less heavily damped than higher order higher frequency modes with $\omega \rightarrow \omega_b$.

In Fig. 9 we display the spatial Landau damping rate predicted by Eq. (34) for the $n=2$ quasimode as a function of $k_{\perp}L$, taking equilibrium density profiles for which $\lambda_D/L=0.075$ (the solid line) and $\lambda_D/L=0.04$ (the dashed line). In the same figure we also display the damping rate ν obtained from fitting an exponentially decaying oscillation to $\delta\langle z^2 \rangle(t)$ in the range $0 < \omega_b t < 100$. For several of the points we also fit only data in the range $50 < \omega_b t < 100$. The difference in the resulting rate indicates that the decay is not

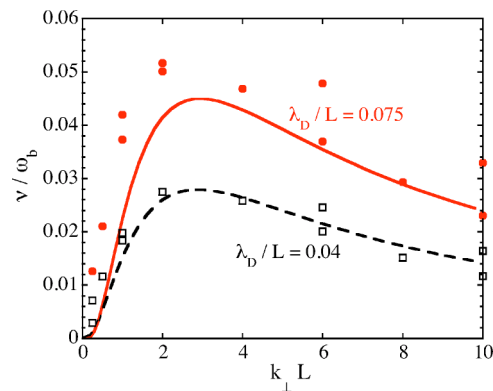


FIG. 9. (Color online). Spatial Landau damping rate ν of the $n=2$ quasimode vs k_{\perp} , assuming cold-fluid dynamics, for two equilibrium density profiles; one with a sharp edge ($\lambda_D/L=0.04$) and one with a broader edge ($\lambda_D/L=0.075$) (see Fig. 3). Lines: Eq. (34). Dots: fits to the decay of $\delta\langle z^2 \rangle(t)$, as in Fig. 7. Squares: $\lambda_D/L=0.04$. Solid circles: $\lambda_D/L=0.075$.

purely exponential at all times. This is expected theoretically since exponential Landau damping is valid only in the time-asymptotic limit. The points match the theory for an equilibrium profile with $\lambda_D/L=0.04$ better than for $\lambda_D/L=0.075$ because in the former case the profile has a sharper density fall-off at the edge, making the assumptions behind Eq. (34) a better approximation.

The preceding eigenmode analysis used cold-fluid theory to evaluate the plasma eigenmodes of continuous density profiles such as that given by the dotted line in Fig. 3. This sort of profile could occur in cold-fluid theory if the background density were due to ions with this nonuniform-density distribution. In the cold-fluid limit electrons would match their density to this profile, and the preceding analysis of the continuous spectrum would apply. However, in a thermal equilibrium non-neutral plasma confined in a Penning trap, n_b is constant and the nonuniform density arises from thermal effects. To properly solve for the modes of a non-neutral plasma, we should include these thermal effects in the eigenmode equation.

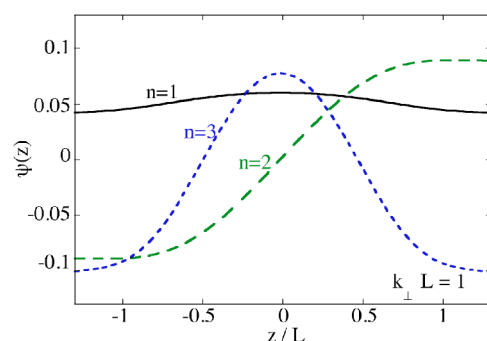


FIG. 10. (Color online). The first three warm-fluid displacement eigenmodes of a thermal equilibrium plasma (see Fig. 3) for $k_{\perp}L=1$, and $\lambda_D/L=0.075$ in both the equilibrium and the dynamics. Corresponding frequencies are shown in Fig. 1.

3. Warm-fluid effects on a continuous profile

The behavior of the displacement eigenmodes changes dramatically when finite temperature-effects are added to the eigenmode equation, which now becomes

$$-\omega^2 \psi(z) = -\omega_p^2(z) \psi(z) + \int dz' \frac{k_{\perp}}{2} e^{-k_{\perp}|z-z'|} \omega_p^2(z') \psi(z') + \bar{v}^2 \left[\frac{\partial^2 \ln n_0}{\partial z^2} \psi(z) + \frac{\gamma}{n_0} \frac{\partial}{\partial z} \left(n_0 \frac{\partial \psi}{\partial z} \right) \right]. \quad (35)$$

We solve this problem numerically using the same finite-difference scheme as before. For the term involving the derivatives of ψ , we use the following difference scheme:

$$\frac{1}{n_0(z)} \frac{\partial}{\partial z} \left(n_0 \frac{\partial \psi}{\partial z} \right) \Bigg|_{z=z_j} = \frac{1}{n_0(z_j)} \left[\frac{n_0(z_j) + n_0(z_{j+1})}{2} \frac{\psi_{j+1} - \psi_j}{\Delta z^2} - \frac{n_0(z_j) + n_0(z_{j-1})}{2} \frac{\psi_j - \psi_{j-1}}{\Delta z^2} \right] \quad (36)$$

which is second-order accurate in Δz , and Hermitian.

We calculate numerical results for $k_{\perp}L=1$ and $\lambda_D/L=0.075$, the same case as we studied previously. The warm-fluid corrections completely change the character of the eigenmodes. The frequency spectrum is again discrete (Fig. 1), and eigenfunctions are no longer singular (Fig. 10). This is because the restoring force from plasma pressure smoothes out rapid density variations in the low-order modes. The mode frequencies increase above the maximum plasma fre-

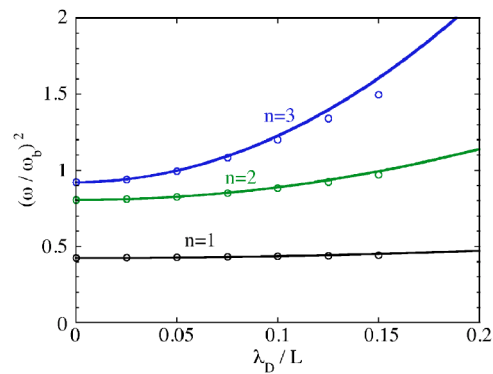


FIG. 11. (Color online). Warm-fluid mode frequencies vs temperature for the first three displacement eigenmodes of a thermal equilibrium plasma, where λ_D is the Debye length associated with both the equilibrium (see Fig. 3) and the dynamics, and assuming $k_{\perp}L=1$. Circles are numerical results, lines are Eq. (37).

quency ω_b as the mode number n increases, also due to the effect of plasma pressure on the modes, as expected qualitatively from Eq. (13) (taking $k_z \propto n/L$ in that equation). For low temperatures, the form of the eigenfunctions is similar to that for zero temperature, as may be seen by comparing Fig. 10 to Fig. 2. There is no spatial Landau damping of these modes. Mode frequencies are shifted upward as temperature increases (Fig. 11).

For low temperatures, one can analytically predict the shift in the mode frequencies¹¹ due to finite temperature. The frequency shift $\Delta\omega$ is predicted to be

$$\Delta\omega = \frac{\omega_0 \lambda_D^2}{2} \frac{\left[\left\langle \nabla^2 \left| \frac{\partial \delta\phi}{\partial z} \right|^2 \right\rangle - \frac{\omega_b^2}{\omega_0^2} \left\langle \frac{\partial^2}{\partial z^2} \left| \frac{\partial \delta\phi}{\partial z} \right|^2 \right\rangle + \frac{\gamma \omega_b^2}{\omega_0^2} \left\langle \left| \frac{\partial^2 \delta\phi}{\partial z^2} \right|^2 \right\rangle \right]}{\left\langle \left| \frac{\partial \delta\phi}{\partial z} \right|^2 \right\rangle}, \quad (37)$$

where ω_0 and $\delta\phi$ are the frequency and potential eigenmode at $T=0$, respectively [given by Eqs. (24) and (25) for slab geometry], and $\langle \rangle$ is a volume average over the interior of the uniform-density zero-temperature plasma. The analytic prediction for $k_{\perp}L=1$ matches the numerically defined frequencies for the lowest modes, provided that λ_D/L is small (Fig. 11).

4. Disappearance of spatial Landau damping

We consider how and why spatial Landau damping disappears when thermal pressure effects are added to the eigenmode equation. We will study the behavior of the system for a *fixed* continuous density profile, given by the dotted line in Fig. 3 (the $\lambda_D/L=0.075$ case), and allow the tempera-

ture T in the eigenmode equation to vary independently. For $T=0$, we obtain the continuous cold-fluid spectrum considered in Sec. III B 2, and for T chosen so that $\lambda_D/L=0.075$ we obtain the discrete spectrum discussed in Sec. III B 3. For intermediate values of T such that $0 < \lambda_D/L < 0.075$ in the eigenmode equation (but fixed density profile), we find that the spectrum is still discrete. An example spectrum is shown in Fig. 4, for $\lambda_D/L=0.01$ and $k_{\perp}L=1$. Although the mode frequencies are closely spaced, their values become independent of M as M increases, at least for those low-order modes with frequencies below ω_b (see the inset to Fig. 4).

As $\lambda_D/L \rightarrow 0$, the spacing $\delta\omega$ between the eigenmodes approaches zero (within numerical resolution). Although individual eigenmodes are not singular for small but finite λ_D/L , they display rapid variation outside the plasma, and so cannot be excited individually by initial conditions for which $\delta Z_0(z)$ is slowly varying in z . Rather, such initial conditions

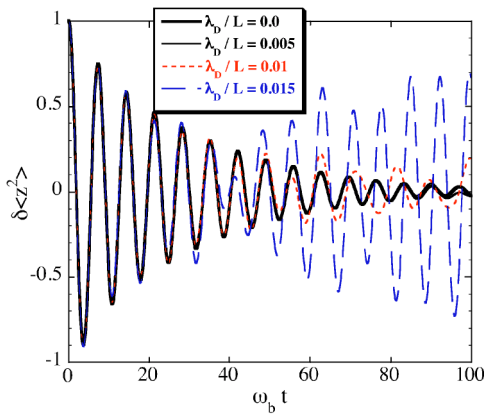


FIG. 12. (Color online). Time evolution of the $n=2$ quasimode for $k_{\perp}L=1$ for four temperatures in the dynamics, keeping the equilibrium density profile fixed (the dotted line in Fig. 3).

excite a range of eigenmodes, just as in the cold fluid limit. This leads to dynamics that is almost indistinguishable from dynamics in the cold fluid limit.

For example, consider the evolution of the same $n=2$ $k_{\perp}L=1$ initial condition as considered previously, in Secs. III B 2 and III B 3. Results for $\delta\langle z^2 \rangle(t)$ are shown in Fig. 12 for several temperatures in the eigenmode dynamics. For very small λ_D/L , say $\lambda_D/L=0.005$, we observe the same behavior as for $T=0$: filamentation and spatial Landau damping of the smooth initial perturbation. This is not surprising since the spacing $\delta\omega$ between modes is so small that the spectrum is nearly continuous. However, as T increases, $\delta\omega$ increases and the time over which spatial Landau damping occurs is reduced; it is as if we have introduced a finite grid error into the response. According to Eq. (33), we expect to see the spatial Landau damping only for times t such that $\delta\omega_m \lesssim 1$, where $\delta\omega_m$ is the maximum spacing between adjacent modes (due now to thermal effects, not numerical grid resolution). This is in fact what our numerical solutions show. For short times, Landau damping occurs as in the $T=0$ case, but for large times the solution no longer decays.

Thus, we expect Landau damping to disappear entirely when $\nu \lesssim \delta\omega_m$, where ν is the Landau damping rate for cold-fluid dynamics. This inequality is well-satisfied when the eigenmode dynamics has the same temperature as the equilibrium. For instance, when $\lambda_D/L=0.075$, $\delta\omega_m/\omega_b \sim 0.2$ (see Fig. 1) but $\nu/\omega_b=0.0374$ (see Fig. 7). This explains why Landau damping was not observed in the warm-fluid results of Sec. III B 3.

5. Kinetic effects

Spatial Landau damping of plasma modes is purely a fluid effect: a quasimode resonantly excites short wavelength plasma waves, filamenting the density (Fig. 8). However, wave-particle resonance can cause filamentation and phase mixing of the *velocity* distribution that induces *kinetic* Landau damping. While the competition between spatial and kinetic Landau damping has been considered in certain geometries,¹⁶ its effect on normal modes of a plasma slab has not been elucidated, to our knowledge.

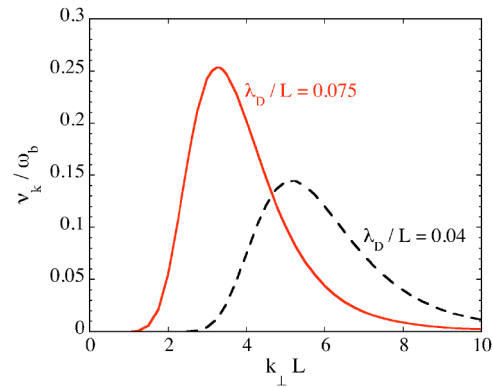


FIG. 13. (Color online). Estimate of the rate of kinetic Landau damping ν_k for the $n=2$ mode (see Fig. 2) for two temperatures, vs perpendicular wave number k_{\perp} ; to be compared to Fig. 9.

Qualitatively, however, one might imagine that kinetic Landau damping would be important if the kinetic Landau damping rate is as large as the spatial Landau damping rate ν , and would not be important otherwise. For a plasma slab calculation of the kinetic rate involves evaluation of multiple bounce resonances in the particle dynamics, and is rather involved. Here, we simply estimate the kinetic rate using the formula for an infinite plasma,

$$\nu_k = \omega \sqrt{\pi/8} \left(\frac{v_{\phi}}{v} \right)^3 e^{-1/2(v_{\phi}/v)^2}, \quad (38)$$

where $v_{\phi} = \omega/k_z$ is the phase velocity of the mode, and we take for k_z the wave number associated with a cold-fluid eigenmode [see Eq. (24)], $k_z = k_{\perp}/\varepsilon(\nu)$. This kinetic damping rate is plotted in Fig. 13 for two values of λ_D/L , as a function of $k_{\perp}L$, for the $n=2$ top-hat mode (see Fig. 2). For $k_{\perp}L \lesssim 1$, ν_k is negligible, and we might then expect to see the effects associated with spatial Landau damping. However, a definite answer to this question must await further calculation.

C. Penning trap geometry, continuous profile, warm-fluid effects

Displacement eigenmodes can also be numerically evaluated for plasmas confined in the cylindrical geometry typical of Penning traps, where the equilibrium density is $n_0 = n_0(\rho, z)$ in cylindrical coordinates. We finite difference Eq. (17) on a uniform rectangular grid in ρ and z ,

$$\rho_j = \Delta\rho(j - 1/2), \quad j = 1, \dots, M \quad (39)$$

$$z_k = -L + (k - 1/2)\Delta z, \quad k = 1, \dots, M$$

where $\Delta z = 2L/M$, and $\Delta\rho = L/(M - 1/2)$. For simplicity we use an $M \times M$ grid in a rectangular region with a fixed aspect ratio of 2:1, but it is easy to generalize to grids with unequal numbers of points in the ρ and z directions and to regions with variable aspect ratio. The warm-fluid part of the

acceleration operator is differenced using the same scheme as in Eq. (36). For the cold-fluid part of the acceleration operator, we note that $G = G(\rho, \rho', |z - z'|)$, and that this function varies rapidly when $\rho \approx \rho'$ and $z \approx z'$. Therefore we use the following difference scheme: writing $\delta Z_{ij} \equiv \delta Z(\rho_i, z_j)$,

$$\mathcal{G}(\rho_i, \rho_k, z_j, z_\ell) \equiv \begin{cases} \frac{\partial^2 G(\rho_i, \rho_k, |z_j - z_\ell|)}{\partial z_j \partial z_\ell}, & \Delta r_{ijk\ell} > 5\Delta\rho \\ \int_{\rho_k - \Delta\rho/2}^{\rho_k + \Delta\rho/2} \rho' d\rho' \int_{z_\ell - \Delta z/2}^{z_\ell + \Delta z/2} dz' \frac{\partial^2 G}{\partial z_j \partial z'}(\rho_i, \rho_k, |z_j - z'|) / \rho_k \Delta\rho \Delta z, & \Delta r_{ijk\ell} < 5\Delta\rho \end{cases} \quad (41)$$

and $\Delta r_{ijk\ell} = \sqrt{(\rho_i - \rho_k)^2 + (z_j - z_\ell)^2}$.

The integral over a grid cell is performed when the relative displacement $\Delta r_{ijk\ell}$ between source and field point is small (less than $5\Delta\rho$), so as to account for the rapid variation of the Green's function in this region. Here the z' integral can be performed analytically via the fundamental theorem of calculus, and in some cases the radial integral can also be performed analytically, depending on the form of the Green's function. The asymmetry in Eq. (41) between field and source points implies that the discretized acceleration operator is not perfectly Hermitian; however as a practical matter the negative consequences of this (i.e., small imaginary components to the frequencies) are far outweighed by the superior accuracy of the discretized integral over source points.

We will concentrate here on free-space boundary conditions where the plasma is far from any boundaries, so that the mode potential vanishes at ∞ . We also specialize to cylindrically symmetric eigenmodes. In this case the Green's function required in Eq. (41) is

$$G(\rho, \rho', z) = -\frac{1}{2\pi^2} \frac{K(-4\rho\rho'/[(\rho - \rho')^2 + z^2])}{\sqrt{(\rho - \rho')^2 + z^2}}, \quad (42)$$

where $K(x)$ is a complete elliptic integral of the first kind (this Green's function is proportional to the potential of a charged ring in free space). An integral equation similar to Eq. (40), also involving this Greens function, has been used by Jenkins and Spencer¹⁷ to study the cold fluid drumhead modes of a plasma disc.

In order to proceed, we must specify an equilibrium density $n_0(\rho, z)$. While any plasma equilibrium could be used, we will concentrate on thermal equilibrium density profiles in free space. These profiles are given by generalizations of Eqs. (30)–(32):

$$n_0(\rho, z) = n_0(0, 0) e^{-[\phi(\rho, z) + \phi_e(\rho, z) - \phi(0, 0) - \phi_e(0, 0) + (1/4)m\omega_b^2\rho^2]}, \quad (43)$$

where $n_0(0, 0)$ is the central density, $\phi_e(\rho, z)$ is the external confinement potential from distant electrodes, and $\phi(\rho, z)$ is the plasma potential that satisfies Poisson's equation

$$(\hat{A}_0 \delta Z)_{ij} = 2\pi \sum_{k\ell} \omega_p^2(\rho_k, z_\ell) \rho_k \Delta\rho \Delta z \mathcal{G}(\rho_i, \rho_k, z_j, z_\ell) \delta Z_{k\ell}, \quad (40)$$

where

$$\nabla^2 \phi = -4\pi e^2 n_0(\rho, z) \quad (44)$$

with the free-space boundary condition that

$$\phi \rightarrow 0 \text{ as } |\mathbf{r}| \rightarrow \infty. \quad (45)$$

For the external potential we choose

$$\phi_e(\rho, z) = \frac{1}{2} m \omega_z^2 (z^2 - \rho^2/2), \quad (46)$$

where ω_z is the axial bounce frequency. With this choice Eqs. (43) and (44) can be combined, writing them as

$$\bar{\nabla}^2 \chi = -\frac{n_0(0, 0)}{n_b} e^{-[\chi(\bar{r}, \bar{z}) - \chi(0, 0) + (\bar{z}^2 + \beta \bar{\rho}^2)/2(2\beta + 1)]}, \quad (47)$$

where $\chi(\bar{\rho}, \bar{z}) = \phi/T$, barred variables are normalized to λ_D , and the trap parameter β is defined as

$$\beta = \frac{1}{2} \left(\frac{\omega_b^2}{\omega_z^2} - 1 \right). \quad (48)$$

Solutions depend on β as well as on $n_0(0, 0)/n_b$. This latter parameter is chosen so that

$$\int d^3r n_0(\rho, z) = N, \quad (49)$$

a fixed particle number as the temperature varies. In general the plasma is a spheroid, prolate for $\beta > 1$ and oblate for $\beta < 1$. In Fig. 14 we show equilibrium density profiles that are solutions of Eq. (47) for the spherically symmetric case β

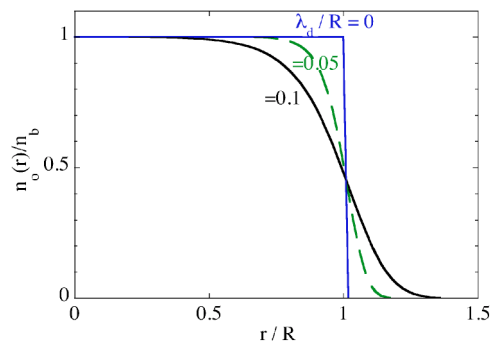


FIG. 14. (Color online). Thermal equilibrium density vs spherical radius r for three temperatures.

TABLE I. Cold-fluid magnetized plasma displacement modes of a sphere.

Mode number	ω/ω_b	$\delta Z(\rho, z)$
(1,0)	$1/\sqrt{3}$	1
(2,0)	$\sqrt{3}/5$	z
(3,0)	$\sqrt{(3 \pm 2\sqrt{6/5})/7}$	$10z^2 - 5[1 - (\omega_b/\omega)^2]\rho^2 - 2R^2(\omega_b/\omega)^2$

= 1. Here the temperature is parametrized by the ratio λ_D/R rather than $n_0(0,0)/n_b$, where R is the cold-fluid radius given by $(4/3)\pi n_b R^3 = N$.

To find accurate eigenfrequencies associated with these density profiles, we require a computational grid that is sufficiently fine to resolve the plasma edge. For low temperatures where $\lambda_D/R \ll 1$, this requires M to be very large. On our current computer system, computational efficiency begins to degrade for $M \geq 60$ (i.e., $M^2 = 3600$ eigenmodes), so this requires $\lambda_D/R \geq 0.035$ (i.e., roughly 2 grid points per Debye length when $M=60$ and $L \approx R$). The numerical method gives M^2 eigenmodes spanning a continuous frequency band from 0 to above ω_b , depending on the temperature T .

For large M values, it can be a painful task to sort the low-order modes of experimental interest out of the set of M^2 eigenmodes. Therefore, it is useful to have some prior knowledge of the mode structure. For example, we can use knowledge of the modes in the cold-fluid limit, where $n_0(\rho, z)$ is constant within the plasma. If the temperature is not too large, these cold-fluid eigenmodes can then be used to determine warm-fluid mode frequencies without needing to compute the eigenmodes of the M^2 by M^2 matrix A_{ij} . If we are looking for the frequency of the warm-fluid version of a given cold-fluid mode $\delta Z_f(\rho, z)$, we can take the inner product of Eq. (16) with respect to this mode:

$$-\omega^2(\delta Z_f, \delta Z) = (\delta Z_f, \hat{A} \delta Z). \quad (50)$$

For low T we may approximate δZ by δZ_f in the equation, obtaining

$$-\omega^2 = \frac{(\delta Z_f, \hat{A} \delta Z_f)}{(\delta Z_f, \delta Z_f)}. \quad (51)$$

The inner products in Eq. (51) can be easily evaluated numerically, using the second-order-accurate finite-difference scheme

$$(f, g) = \sum_{j,k} \omega_p^2(\rho_j, z_k) \rho_j f^*(\rho_j, z_k) g(\rho_j, z_k) 2\pi \Delta \rho \Delta z \quad (52)$$

for any two functions $f(\rho, z)$, $g(\rho, z)$. Equation (51) allows us to obtain eigenfrequencies for low-order modes over a range of temperatures, including the range $\lambda_D/R < 0.05$. However, its use requires knowledge of the cold fluid modes for the given equilibrium.

Fortunately, the cold fluid-eigenmodes of a spheroidal plasma in free space are known analytically.¹⁸ Table I provides the functional forms of some of the low-order cylindrically symmetric plasma modes. Modes are enumerated by two integers (ℓ, m) , where m is the azimuthal mode number

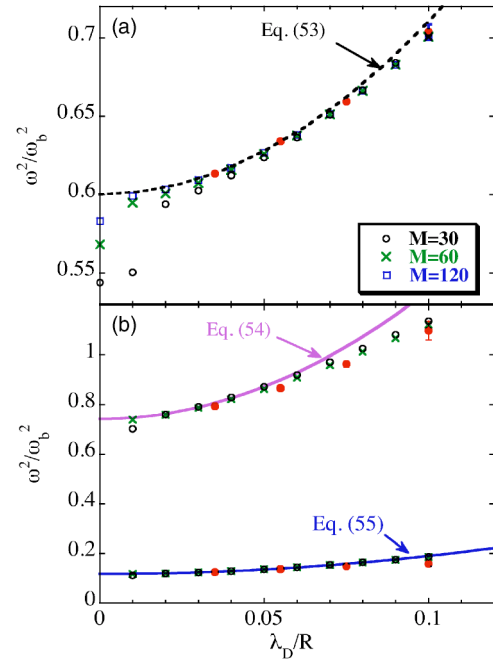


FIG. 15. (Color online). Warm-fluid mode frequency vs temperature in a spherical plasma, where λ_D is the Debye length associated with both the equilibrium (see Fig. 14) and the dynamics, and R is the cold-fluid plasma radius. Open circles, crosses, and squares are results of Eq. (51) at different resolutions. Solid circles are obtained from a fit to the plasma evolution, discussed in the text. (a) (2,0) mode; (b) (3,0) modes.

and ℓ is the axial mode number. The integer $|m|$ counts the number of zeros in the potential around the equator of the spheroid, and $\ell - |m|$ is the number of zeros encountered as one traverses a great circle from pole to pole. For $m=0$ (i.e., azimuthally symmetric modes), there are $1 + \text{Int}[(\ell-1)/2]$ plasma modes for a given value of ℓ , each with different radial and axial variation. For the (1,0) mode, Eq. (51) can be evaluated analytically to obtain $\omega^2 = \omega_z^2$, independent of temperature, as expected for the center-of-mass mode in a plasma in a harmonic confinement potential.

For the spherical case $\beta=1$, the frequency as a function of temperature is plotted in Fig. 15 for the (2,0) and (3,0) modes, determined using Eq. (51). When λ_D/R is small, the grid must be very fine in order to obtain well-converged results; we use up to $M=120$ in the computations involving Eq. (51) (the open circles, crosses, and squares). The (2,0) and (3,0) modes display thermal frequency shifts that are in good agreement with the frequencies expected from Eq. (37) and Table I:

$$\left(\frac{\omega_{2,0}}{\omega_b}\right)^2 = \frac{3}{5} + 11 \frac{\lambda_D^2}{R^2}, \quad (53)$$

$$\left(\frac{\omega_{3,0}^{(1)}}{\omega_b}\right)^2 = 0.7415 + 51.683 \left(\frac{\lambda_D}{R}\right)^2, \quad (54)$$

$$\left(\frac{\omega_{3,0}^{(2)}}{\omega_b}\right)^2 = 0.1156 + 7.317 \left(\frac{\lambda_D}{R}\right)^2. \quad (55)$$

(Note that these results hold only for a spherical plasma. More general expressions can be found in Ref. 11.)

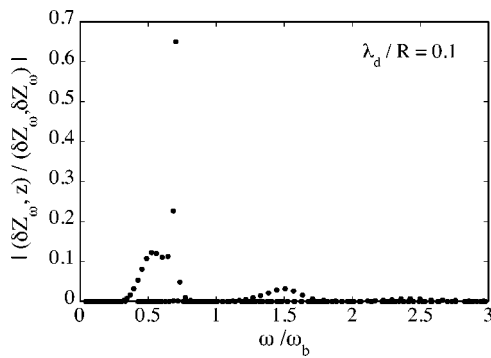


FIG. 16. Warm-fluid excitation spectrum in a spherical plasma vs frequency for (2,0)-type initial condition $\delta Z_0 = z$, assuming $\lambda_D/R = 0.1$ in both the dynamics and the equilibrium.

However, this agreement should not be taken as suggesting that the spectrum is discrete. Surprisingly, the warm-fluid eigenmodes obtained directly from Eqs. (16), (17), (36), and (40) again exhibit a continuous spectrum, and result in spatial Landau damping of initial perturbations. This can be seen in several ways: from examining evolution of an initial condition that displays Landau damping, from the singular form of the eigenmodes, and from filamentation of the density at a resonance layer.

First, we determine the overlap of the eigenmodes with a given low-order fluid mode, choosing for this example the (2,0) mode where $\delta Z_f = z$. The excitation spectrum $(\delta Z_\omega, z) / (\delta Z_\omega, \delta Z_\omega)$ for $\lambda_D/R = 0.1$ is shown in Fig. 16 as a function of frequency, using a 40 by 40 grid in ρ and z . Although there is a sharp peak in this spectrum near the expected fluid frequency of $\omega_0 = \sqrt{3/5}\omega_b$, there is also broadening of the spectrum. As a result, when this spectrum is used to evaluate the initial value problem given by Eq. (19), one finds that global measures of the perturbation amplitude such as $\langle z^2 \rangle(t)$ decay with time (Fig. 17). Also, the eigenmodes that contribute to the peak of the excitation spectrum have a singularity at $\rho \approx 1.2R$, as would be expected for the singular eigenmodes associated with a continuous spectrum (Fig. 18). However, the functional form and the location of this singularity is not yet understood. It is presumably connected in some way to a resonance condition such as

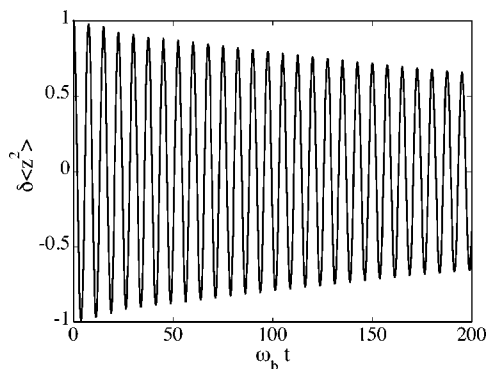


FIG. 17. Time evolution of $\delta \langle z^2 \rangle(t)$ in a spherical plasma, arising from the excitation spectrum of Fig. 16.

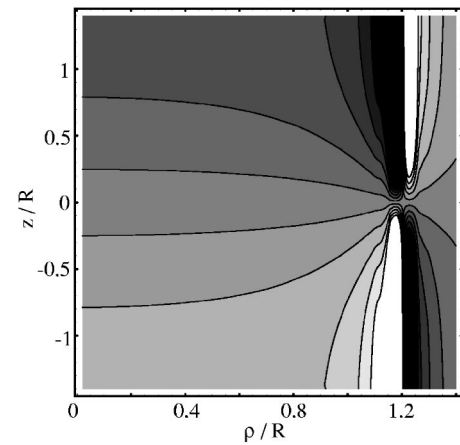


FIG. 18. Contour plot in the ρ - z plane of the warm-fluid eigenmode at the peak of the spectrum shown in Fig. 16.

$\omega_p(\rho, z) = \omega_0$. However, this condition would yield a singular surface at a spherical radius $r = 0.87R$, not at $\rho = 1.2R$.

We can directly observe the filamentation of the density profile caused by spatial Landau damping, by following $\delta Z(\rho, z, t)$ as it evolves according to Eq. (19). Surface plots of $\delta Z(\rho, z, t)$ are shown in Fig. 19 three times. It appears that the filamentation is associated with the resonant emission of plasma waves with long axial wavelength and progressively shorter radial wavelength as time evolves. The long axial wavelength of the waves implies that warm-fluid theory remains valid throughout the filamentation process. These waves are centered around $\rho = 1.2R$ and travel toward smaller radius. This may be seen in Fig. 20, which plots contours of $\delta Z(\rho, z = 0.5R, t)$. The negative slope of the contours at $\rho = 1.2R$ indicates waves traveling radially inward. Also, one can see that the intensity of these waves increases with time, as at a resonance.

The overall frequency of the mode, as determined by a fit to the data displayed in Fig. 17, matches the results of the perturbation calculations. This can be seen in Fig. 15(a), where the frequency determined in this manner is given by the closed circle at $\lambda_D/R = 0.1$. The error bars reflect the uncertainty in the frequency caused by the damping. The calculation was repeated for several values of λ_D/R , and for the two (3,0) modes, as shown by the other closed circles in Fig. 15. In every case, the frequency follows the results of Eqs. (53)–(55) within the error.

IV. DISCUSSION

We have seen that displacement eigenmodes provide a straightforward numerical method for evaluating both the cold- and warm-fluid magnetized plasma dynamics of perturbations around a variety of plasma equilibria. Several aspects of the eigenmodes could be understood theoretically: for instance, frequency shifts of the modes due to warm-fluid effects were found to agree with previously calculated shifts.¹¹ This is actually rather surprising since the previous analytic theory involved approximations that appeared to restrict the results to strongly correlated plasmas. Furthermore, in slab

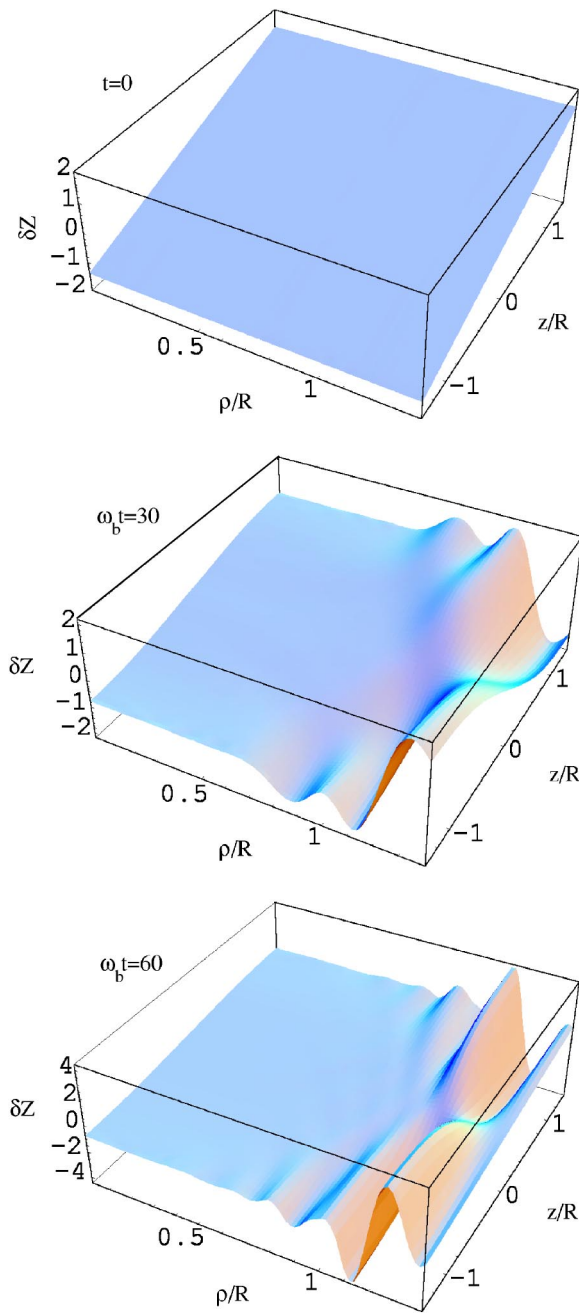


FIG. 19. (Color online). Surface plots of $\delta Z(\rho, z, t)$ at three times, for a spherical plasma with $\lambda_D/R=0.1$ in both the equilibrium and dynamics. Initially, $\delta Z=z$.

geometry and in the cold-fluid limit, spatial Landau damping of initial perturbations was observed and connected to the well-known theory of collisionless fluid damping due to resonant excitation of short-wavelength plasma waves.

However, other aspects of our numerical results still require theoretical explanation. For spherical plasmas, we observed spatial Landau damping that also appears to be due to a fluid resonance; but the form of the resonance is not understood. Another related issue that remains to be fully addressed is the addition of kinetic effects to the theory, which will allow additional collisionless damping due to direct wave-particle resonance. In future work we intend to study these issues in plasmas with different shapes and density

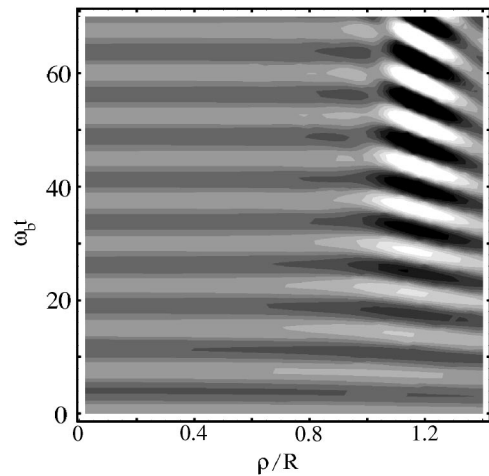


FIG. 20. Contour plot of $\delta Z(\rho, z=0.5R, t)$ for same evolution as shown in Fig. 19.

profiles, especially finite-length cylindrical columns, and to compare the theory results to actual experimental data.¹⁹

ACKNOWLEDGMENTS

This work was supported by the National Science Foundation and the Department of Energy under Grant No. PHY0354979.

APPENDIX A: LAPLACE TRANSFORM APPROACH TO COLLISIONLESS DAMPING OF COLD-FLUID MAGNETIZED PLASMA WAVES

In this appendix we review the cold-fluid theory for spatial Landau damping of collisionless magnetized plasma waves in slab geometry, for an arbitrary equilibrium density profile $n_0(z)$, assuming only that $n_0(z) \rightarrow 0$ as $z \rightarrow \pm\infty$. By Laplace-transforming the linearized versions of Eqs. (1)–(3), we obtain the following equations for evolution of the perturbed potential, which is of the form $e^{i\mathbf{k}\cdot(\mathbf{x},y)} \delta\phi(z, t)$:

$$\delta\phi(z, t) = \int_C \frac{ds}{2\pi i} e^{st} \delta\hat{\phi}(z, s), \quad (\text{A1})$$

where s is the Laplace transform variable, the contour C runs from $-i\infty$ to $i\infty$, to the right of all poles in $\delta\hat{\phi}(z, s)$, and where the Laplace transform function $\delta\hat{\phi}(z, s)$ satisfies

$$\frac{\partial}{\partial z} \left[\left(1 + \frac{\omega_p^2(z)}{s^2} \right) \frac{\partial \hat{\phi}}{\partial z} \right] - k_{\perp}^2 \delta\hat{\phi} = F(z, s). \quad (\text{A2})$$

Here $F(z, s) = -(\partial/\partial z)(4\pi en_0[s\delta Z_0(z) + \delta V_0(z)]/s^2)$, where δZ_0 and δV_0 are initial fluid displacement and velocity, respectively. Equation (A2) can be solved using a Green's function to yield

$$\begin{aligned} \delta\hat{\phi}(z,s) = & -\delta\hat{\phi}_1(z,s) \int_z^\infty dz' \frac{F(z',s)\delta\hat{\phi}_2(z',s)}{W(z',s)} \\ & -\delta\hat{\phi}_2(z,s) \int_{-\infty}^z dz' \frac{F(z',s)\delta\hat{\phi}_1(z',s)}{W(z',s)}, \end{aligned} \quad (\text{A3})$$

where $\delta\hat{\phi}_1$ and $\delta\hat{\phi}_2$ are solutions to the homogeneous equation ($F=0$) with boundary conditions that $\delta\hat{\phi}_1(z=-\infty)=0$ and $\delta\hat{\phi}_2(z=+\infty)=0$, and where $W=\delta\hat{\phi}_1'\delta\hat{\phi}_2-\delta\hat{\phi}_2'\delta\hat{\phi}_1$ is the Wronskian.

Spatially Landau-damped quasimodes appear as poles in $\delta\hat{\phi}(z,s)$. By deforming the contour in Eq. (A1) around these poles [i.e., moving it to the left into the $\text{Im}(s)<0$ half plane], the behavior of $\delta\hat{\phi}$ at large times can be shown to be dominated by the pole with the smallest real part, $s_0=-i\omega_0-\nu$:

$$\lim_{t\rightarrow\infty} \delta\phi(z,t) = \mathcal{R}e^{s_0 t}, \quad (\text{A4})$$

where \mathcal{R} is the residue of $\delta\hat{\phi}(z,s)$ at $s=s_0$. According to Eq. (A3), poles in $\delta\hat{\phi}$ occur where the Wronskian vanishes, and this in turn occurs where $\delta\hat{\phi}_1$ and $\delta\hat{\phi}_2$ are no longer independent, i.e., at values of s where there is a nontrivial solution to

$$\frac{\partial}{\partial z} \left[\left(1 + \frac{\omega_p^2(z)}{s^2} \right) \frac{\partial \delta\hat{\phi}}{\partial z} \right] - k_\perp^2 \delta\hat{\phi} = 0, \quad \delta\hat{\phi} = 0 \text{ at } z = \pm\infty. \quad (\text{A5})$$

Values of s for which this equation is satisfied nontrivially provide the quasimode frequencies. Such solutions are found by deforming the z integration in Eq. (A5) below the singularity in this equation at $\omega_p^2(z)=-s^2$, so as to analytically continue $\delta\hat{\phi}$ from the $\text{Im}(s)>0$ half plane to the $\text{Im}(s)<0$ half plane.

Analytic equations for the quasimode frequencies can be found when $\nu/\omega_b \ll 1$. By integrating twice, Eq. (A5) can be expressed as

$$\begin{aligned} \delta\hat{\phi}(z) = & \delta\hat{\phi}(z_{\text{out}}) - \int_z^{z_{\text{out}}} \frac{dz'}{1 + \frac{\omega_p^2(z')}{s^2}} \left[\delta\hat{\phi}'(z_{\text{out}}) \right. \\ & \left. + k_\perp^2 \int_{z_{\text{out}}}^{z'} dz'' \delta\hat{\phi}(z'') \right], \end{aligned} \quad (\text{A6})$$

where z_{out} is a point outside the plasma and where the integration contours must proceed below the pole where $s^2 + \omega_p^2(z')=0$, taking $s=-i\omega_0-\nu$. For $\nu/\omega_0 \ll 1$, we can apply the Plemelj formula to obtain

$$\begin{aligned} \delta\hat{\phi}(z) = & \delta\hat{\phi}(z_{\text{out}}) + i\pi \int_z^{z_{\text{out}}} dz' \delta \left(1 - \frac{\omega_p^2(z')}{\omega_0^2} \right) \left[\delta\hat{\phi}'(z_{\text{out}}) \right. \\ & \left. + k_\perp^2 \int_{z_{\text{out}}}^{z'} dz'' \delta\hat{\phi}(z'') \right] - P \int_z^{z_{\text{out}}} \frac{dz'}{1 - \frac{\omega_p^2}{\omega_0^2}} \left[\delta\hat{\phi}'(z_{\text{out}}) \right. \\ & \left. + k_\perp^2 \int_{z_{\text{out}}}^{z'} dz'' \delta\hat{\phi}(z'') \right], \end{aligned} \quad (\text{A7})$$

where P denotes the principal part of the integral.

For the case of a density profile with a rather sharp edge, as in the thermal equilibrium profiles considered in Sec. III, Eq. (A7) provides a simple jump condition on the potential inside and outside the plasma. Taking $z_{\text{out}}=L+\varepsilon$ and $z_{\text{in}}=L-\varepsilon$ where $\varepsilon=0(\lambda_D)$ is sufficiently large to take us beyond the edge region of the profile but $\varepsilon \ll L$, we can approximate Eq. (A7) as

$$\delta\hat{\phi}(z_{\text{in}}) = \delta\hat{\phi}(z_{\text{out}}) + i\pi \delta\hat{\phi}'(z_{\text{out}}) \int_{z_{\text{in}}}^{z_{\text{out}}} dz' \delta \left(1 - \frac{\omega_p^2(z')}{\omega_0^2} \right). \quad (\text{A8})$$

This result, combined with the standard jump condition on $\delta\hat{\phi}'$ at the plasma edge

$$\left(1 + \frac{\omega_p^2}{s^2} \right) \delta\hat{\phi}'(z_{\text{in}}) = \delta\hat{\phi}'(z_{\text{out}}), \quad (\text{A9})$$

provides us with quasimode frequencies. Inside the plasma $\delta\hat{\phi}$ takes the form of Eq. (24); and outside it takes the form $e^{-k_\perp|z|}$. When these forms are substituted into Eqs. (A8) and (A9) and the integral over the δ function is performed, a nontrivial solution is obtained only if Eq. (34) is satisfied.

¹N. A. Krall and A. W. Trivelpiece, *Principles of Plasma Physics* (San Francisco Press, San Francisco, 1986).

²S. N. Rasband and R. L. Spencer, *Phys. Plasmas* **10**, 948 (2003).

³J. K. Jennings, R. L. Spencer, and K. C. Hansen, *Phys. Plasmas* **2**, 2630 (1995).

⁴N. G. Van Kampen, *Physica (Amsterdam)* **21**, 949 (1955).

⁵K. M. Case, *Phys. Fluids* **3**, 143 (1960).

⁶D. E. Baldwin and D. W. Ignat, *Phys. Fluids* **12**, 697 (1969).

⁷D. E. Baldwin and A. N. Kaufman, *Phys. Fluids* **12**, 1526 (1969).

⁸D. E. Baldwin, D. M. Henderson, and J. L. Hirshfield, *Phys. Rev. Lett.* **20**, 314 (1968).

⁹M. D. Tinkle, R. G. Greaves, and C. M. Surko, *Phys. Plasmas* **2**, 2880 (1995).

¹⁰M. Amoretti, C. Amsler, G. Bonomi *et al.*, *Phys. Rev. Lett.* **91**, 055001 (2003).

¹¹D. H. E. Dubin, *Phys. Rev. E* **53**, 5268 (1996).

¹²T. Stix, *Theory of Plasma Waves* (McGraw-Hill, New York, 1962), p. 36.

¹³D. H. E. Dubin and T. M. O'Neil, *Rev. Mod. Phys.* **71**, 87 (1999).

¹⁴F. Anderegg, N. Shiga, J. R. Danielson, D. H. E. Dubin, and C. F. Driscoll, *Phys. Rev. Lett.* **90**, 115001 (2003).

¹⁵D. A. Schechter, D. H. E. Dubin, A. C. Cass, C. F. Driscoll, I. M. Lansky, and T. M. O'Neil, *Phys. Fluids* **12**, 2397 (2000).

¹⁶See, for example, D. E. Baldwin, *Phys. Fluids* **12**, 279 (1969).

¹⁷T. G. Jenkins and R. L. Spencer, *Phys. Plasmas* **9**, 2896 (2002).

¹⁸D. H. E. Dubin, *Phys. Rev. Lett.* **66**, 2076 (1991).

¹⁹J. R. Danielson, F. Anderegg, and C. F. Driscoll, *Phys. Rev. Lett.* **92**, 245003 (2004).